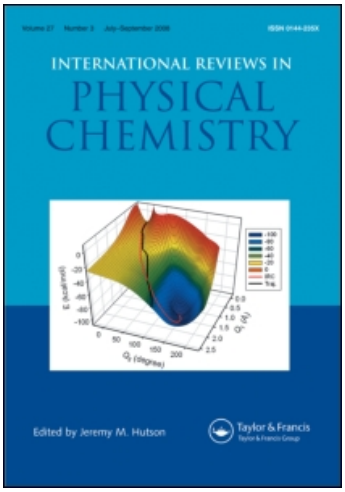


**International Reviews in Physical Chemistry**
Publication details, including instructions for authors and subscription information:
http://www.informaworld.com/smpp/title~content=t713724383

# Computer simulations of structures, energetics and dynamics of myoglobin ··· ligand complexes

Jonas Danielsson[a]; Polina Banushkina[a]; David R. Nutt[a]; Markus Meuwly[a]
[a] Department of Chemistry, CH-4056 Basel, Switzerland

**To cite this Article** Danielsson, Jonas , Banushkina, Polina , Nutt, David R. and Meuwly, Markus(2006) 'Computer simulations of structures, energetics and dynamics of myoglobin ··· ligand complexes', International Reviews in Physical Chemistry, 25: 3, 407 — 425
**To link to this Article: DOI:** 10.1080/01442350600798253
**URL:** http://dx.doi.org/10.1080/01442350600798253

*International Reviews in Physical Chemistry*,
Vol. 25, No. 3, July–September 2006, 407–425

Taylor & Francis
Taylor & Francis Group

# Computer simulations of structures, energetics and dynamics of myoglobin · · · ligand complexes

JONAS DANIELSSON, POLINA BANUSHKINA,
DAVID R. NUTT and MARKUS MEUWLY*

Department of Chemistry, Klingelbergstrasse 80, CH-4056 Basel, Switzerland

(*Received 16 December 2005; in final form 10 May 2006*)



Myoglobin has been studied in considerable detail using different experimental and computational techniques over the past decades. Recent developments in time-resolved spectroscopy have provided experimental data amenable to detailed atomistic simulations. The main theme of the present review are results on the structures, energetics and dynamics of ligands (CO, NO) interacting with myoglobin from computer simulations. Modern computational methods including free energy simulations, mixed quantum mechanics/molecular mechanics simulations, and reactive molecular dynamics simulations provide insight into the dynamics of ligand dynamics in confined spaces complementary to experiment. Application of these methods to calculate and understand experimental observations for myoglobin interacting with CO and NO are presented and discussed.

## Contents



*Corresponding author. Email: m.meuwly@unibas.ch

*International Reviews in Physical Chemistry*
ISSN 0144–235X print/ISSN 1366–591X online © 2006 Taylor & Francis
http://www.tandf.co.uk/journals
DOI: 10.1080/01442350600798253

## 1. Introduction

The investigation of structural and dynamical properties of myoglobin (Mb) has a long history in biophysical chemistry and biophysics. Starting from the early structural work carried out by Kendrew and coworkers [1], Mb has served as a reference system. This can also be explained by its paramount role in physiological processes. Mb is a small globular heme protein that is primarily involved in storing and transporting oxygen ($O_2$) in muscle tissue. However, in recent years interactions of Mb and its mutants with NO as a ligand have been studied both experimentally and theoretically [2–7] due to the physiological importance of nitric oxide. In particular, attention has recently been focused on the interaction of NO with heme proteins because of the wide range of biological functions of this ligand [8]. NO is a key biological messenger which is involved in numerous physiological processes, such as inhibition of mitochondrial respiration, inhibition of the enzyme ribonucleotide reductase and neurotransmission in the brain [9–11]. In many cases NO binding to iron atoms in both heme and non-heme proteins seems to be involved.

The earliest experimental investigations of reactions between Mb and small molecules, however, have focussed on the interaction with CO [12] and between hemoglobin and CO [13]. They used flash photolysis to monitor the dissociation and rebinding of the ligand. Pioneering studies by Austin and coworkers extended the earlier work in temperature, time and dynamic range [2]. These studies found a number of barriers that a ligand rebinding from the solvent has to overcome in approaching the heme docking site. The barriers were found to differ for CO and $O_2$. In part, these different barriers were used to explain that, despite a 30 000 fold increased affinity of CO over $O_2$ to free heme, the binding of $O_2$ to Mb under physiological conditions is greatly enhanced. Further progress was made by improving the time resolution. Cornelius and coworkers used picosecond time resolution to investigate the relaxation in nitrosylhemoglobin [14]. By using infrared radiation, more details of the ligand motion after photodissociation could be examined. It was found that, upon dissociation, CO moves rapidly to the docking site where it remains on the ns time scale. From there, the ligand can either rebind (geminate rebinding), or diffuse further through the protein matrix [15]. Further improvements and new technologies finally allowed to measure the infrared spectrum of photodissociated CO in Mb [16], and determine parts of the ligand pathway after photodissociation [17]. Experiments on Mb interacting with ligands have also been carried out in the liquid phase [18]. A variety of activation sources can be used to investigate the response of the protein to an external perturbation. These include, for example, optical studies (UV, infrared) or electron spin resonance (ESR). Structural questions can be addressed using X-ray crystallography. Recently, the combination of several methods (e.g. time-resolved X-ray crystallography coupled to infrared spectroscopy) [17] or further development of established methods (ultrafast X-ray diffraction) [19] have provided new and exciting insight into the dynamics of Mb. Other developments include the application of temperature derivative spectroscopy (TDS) with well defined heating and cooling protocols [20] that allow to populate particular locations (internal cavities such as the Xe pockets [21]) of the protein after photodissociation. Subsequently, the ligand's properties and environment is interrogated with conventional infrared radiation.

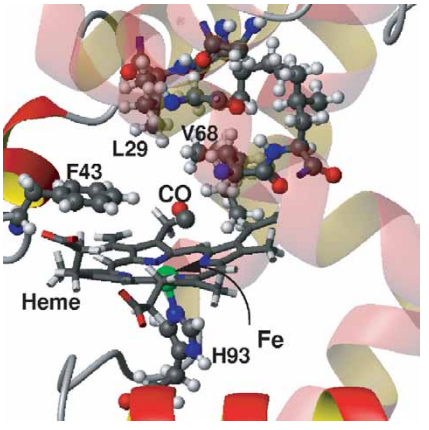


Figure 1. Overview of the active site of myoglobin. The Fe atom (green) is at the centre of the heme group (wire frame), surrounded by different protein residues (in ball and stick) and the 8 helices (indicated by ribbons). The ligand (CO) is photodissociated and the Fe atom is seen to be below the average heme plane. The Fe is covalently bound to the proximal histidine, His93.



Mb is an ideal protein for detailed computer simulations since its size is moderate (153 amino acids, see figure 1) and some of the biologically relevant processes occur on very fast timescales. A typical experiment is the photodissociation of the ligand in which the Fe–C or Fe–N bond is broken using a laser pulse [16]. After the dissociation, the ligand (CO or NO) moves very rapidly (ps) to a docking site where it remains for extended periods of time, particularly for CO. Subsequent migration to nearby protein pockets (the so-called Xe pockets [21]) happens on the ns time scale which is still within reach of atomistic computer simulations. Valuable experimental investigations report corresponding data on native and mutant Mb. Often, point mutations lead to small, but important local changes in the protein environment. If the ligand (CO or NO) is considered to be a probe for the protein environment, simulations for the native and the mutated protein can give detailed information about the quality of the atomistic model used. This is even more relevant since all-atom simulations use conventional force fields [22–25] that can be expected to correctly describe the average behavior of a protein but not necessarily finer details. Thus, to a certain degree the most meaningful molecular dynamics simulations are carried out for systems where differences in quantities upon small, controllable changes can be monitored. Examples include differences in binding energies for a ligand to the native vs. mutant protein, or structural changes in going from the native to a mutant protein.

In the present review recent advances in the understanding of the structure, energetics, spectroscopy and dynamics of Mb with the ligands CO and NO are presented. Section 2 discusses computational methodologies that are used for such investigations while in section 3 results of computer simulations are summarized and compared with experiments. Also, extensions to established simulation methods are described. A short summary and outlook conclude the review.

## 2. Computational methods

Computational work on elucidating and understanding particular observations on myoglobin (and other proteins) can be largely divided into two categories: all-atom simulations and simulations based on some reduction of the number of degrees of freedom. In the latter, selected degrees of freedom are described using more or less elaborate models while implicitly averaging over the remaining degrees of freedom. They include coarse-grained models (which became popular recently) [26], or approaches that are primarily used to extract kinetic data from experiment [27]. In the first approach, a force field is used to describe all internal degrees of freedom. With this force field, molecular dynamics (MD) or Monte Carlo (MC) simulations can be run. Subsequently, the trajectories or configurations are analyzed to calculate experimental observables of interest.

### 2.1. *Molecular dynamics simulations of complex systems*



Computer simulations, and in particular molecular dynamics simulations, have become an important tool to investigate structural, dynamical and kinetic aspects of complex, high-dimensional systems [28, 29]. Conventional MD simulations use a parametrized force field and propagate the Newtonian equations of motion starting from a set of initial coordinates and (typically) random velocities [30]. Combined with special techniques, such as umbrella sampling [31] or thermodynamic integration [32] a variety of observables relevant to experimental work can be calculated.

Owing to the increased computational power available, improvements in treating the intermolecular interactions beyond a conventional force field description become possible. One possibility is mixed quantum mechanical/classical mechanical studies [33–35]. QM/MM simulations have been used for investigations of biologically relevant systems [36]. They decompose the system into a part that is directly involved in the reaction and treat it by quantum mechanics, while the rest of the system is treated by a molecular mechanics force field. Examples for the QM part are explicit *ab initio* techniques (see, e.g. [37]) density functional theory, semiempirical treatments (e.g. AM1 or PM3), empirical valence bond theory (EVB) [38] or approximate valence bond theory (AVB) [39]. However, even in the QM/MM framework high level QM approaches are difficult to use due to the large amount of computer time required for dynamical studies [40]. Yet another, although related, approach is to propagate the nuclear and electronic degrees together, which is the method pioneered by Car and Parrinello [41]. Typically, such calculations are carried out at the density functional level of theory (typically B3LYP for QM/MM and BLYP for Car–Parrinello), because each time step requires the integration of the electronic Schrödinger equation, either with an atomic basis set (QM/MM) or with a plane wave expansion of the total electronic wavefunction and possibly pseudopotentials [41].

Further improvements in force fields concern the inclusion of polarizability and fluctuating charges [42] to describe the adaptation of a charge distribution to changes in the environment. With point charges assigned to atoms it is not possible to correctly represent the electrostatic potential of a molecule. For example, with two point charges for the C and the O atom in carbon monoxide it is possible to describe the zeroth

(total charge $Q$) and first (electrical dipole $\mu$) moment. However, at the equilibrium separation of isolated CO ($r_e = 1.14\,\text{Å}$) $Q = 0$ and $\mu = 0.06\,ea_0$, which is very small. The first not nearly vanishing moment in CO is the quadrupole moment $\Theta = -1.47\,ea_0^2$ which can only be captured with a third point charge. This can either be placed at the geometric or the mass centre of CO. In the particular case of CO high level *ab initio* calculations have shown that the dipole moment changes its sign around the equilibrium separation [43]. Thus, $\mu(r)$ is a function of the CO separation $r$ which changes sign even for the ground vibrational state. These considerations have led to the development of fluctuating and distributed point charge models [44].

Conventional force fields are useful to capture the structure of a protein and fluctuations around it (such as experienced in NMR experiments or normal mode vibrations). However, they are not designed (nor intended) to correctly describe finer details such as the free energy difference between two thermally accessible states. In such a case it is possible to remove particular terms from the force field and replace them with a representation based on DFT or *ab initio* calculations. Such locally improved (in quality) force fields combine the advantages of a conventional force field (rapid evaluation of energies and forces, correct description of the overall geometry of a complex system) with the quantitatively correct aspects of DFT or *ab initio* calculations for reaction barriers or vibrational frequencies.



## 3. Results from computer simulations in the light of experiment

### 3.1. *Structural features*

The crystallographic structure of native, unligated Mb was solved in 1958 [1]. Also, Mb was one of the first proteins for which the structure of a transient species could be solved [45, 46]. This structure concerned photodissociated Mb · CO and directly showed for the first time that CO occupies a metastable position above the heme plane, some 3.5 Å away from the primary binding site, the so-called docking site B. The structure also showed, as earlier studies on photodissociated Mb already had indicated, that after photodissociation of the ligand, the Fe atom sinks into the heme plane by about 0.4 Å and leads to so-called heme-doming. This structural change is – in part – responsible for the observed barrier for rebinding of CO to the heme. To restore the Fe–CO bond after dissociation, the Fe atom has to move back to the heme plane to allow bond formation. Thus, the heme-doming mode has been suggested to be a primary gating-mode to control the rebinding reaction [47].

Molecular dynamics simulations have been carried out for photodissociated CO in Mb using the fluctuating point charge model [44]. From the trajectories it is possible to investigate the localization of the ligand which can be represented as distribution functions as shown in the lower part of figure 2. In the A state (with three spectroscopically distinct substates $A_0$, $A_1$ and $A_3$) CO is bound to Mb (MbCO) while the B state corresponds to photodissociated CO. The B state is located between two pyrrole rings of the porphyrin, and lined by residues L29, F46, H64, T67, V68, and I107 (see figure 1). The maximum of the probability distribution is consistent with the experimental observations [45, 46]. In detailed MD simulations it was found that the

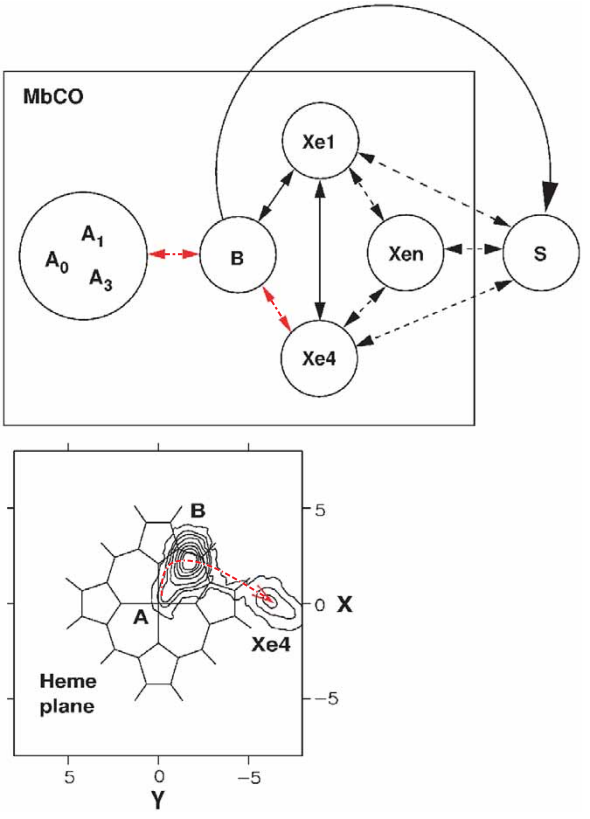


Figure 2. Different CO rebinding paths between the bound states (A), the docking site (B) and various internal cavities (Xe1, Xe4 and Xe*n* (i.e. Xe2 and Xe3)). Solid lines indicate migration paths that have been observed directly by experiment, the (- - -) arrows indicate the path followed in the umbrella sampling path (lower part of figure), and (- - -) lines are further possible pathways. They include the A ↔ B ↔ Xe4 (for L29W) [27], the A ↔ B ↔ Xe4 ↔ Xe1 ↔ B ↔ A (for native Mb) [51, 80], the calculated A ↔ B ↔ Xe4 ↔ Xe3 (for native Mb, via ghost states) ↔ Xe1 ↔ Xe2 ↔ Xe1 [52], and the A↔B↔Xe1 (for native Mb) [77]. Scott *et al.* have proposed a side-path scheme for $MbO_2$ for which A ↔ B ↔ C competes with A ↔ B ↔ S and C is not specified [103, 104]. The lower part of the figure shows an escape path from A via B to Xe4 from MD simulations. Free energy profiles (such as the ones shown in figure 5) are one-dimensional projections including all protein coordinates.

CO molecule can be localized to various degrees, depending on motions of the protein environment. Previous simulations, which used the original three-point charge model [48], found probability distributions that were spatially more restrained [49, 50].

From figure 2 it can also be seen that escape to neighboring pockets (here Xe4) is only possible if the protein motions are sufficiently large. The Xe4 pocket is known to be populated by dissociated ligands and is defined through residues G25, I28, L29, G65, V68, L69, L72, I107, and I111. CO was found in the Xe4 pocket in recent experiments [51] and in atomistically detailed MD simulations [44, 52]. In particular, the pathways discovered from simulations suggested that photolysed CO migrates from

the docking site (B) *via* the Xe4 pocket either further into other binding sites of Mb, or back to B from where it can rebind. Thus, MD simulations are useful to investigate metastable, transient states of ligands after photodissociation.

### 3.2. *Interaction between ligands and protein*

Depending on the atomistic detail required, models of varying complexity may be needed to describe the protein–ligand interaction. In the bound state (MbXO for X = C and N) the Fe–X and the Fe–X–O coordinates are typically described with a harmonic model while for the X–O stretching motion either harmonic or anharmonic potential energy functions have been used [7, 53, 54]. Recently, two-dimensional potential energy functions have been presented for bound MbCO [55] and MbNO [56]. Both potential energy functions were fitted to analytical functions suitable for molecular dynamics simulations. For MbNO the two coordinates included the Fe–CoM(NO) distance (where CoM is the centre of mass of NO) and the angle between the Fe–CoM(NO) and the NO vector. The functional form consisted of an angular expansion in Legendre polynomials and radial strength functions $V_\lambda(R)$

$$V(R,\theta) = \sum_{\lambda=0}^{10} V_\lambda(R) P_\lambda(\cos\theta). \tag{1}$$

The $V_\lambda(R)$ were represented by Morse functions which lead to an overall satisfactory fit of the PES, to within 1 kcal/mol of the energies from DFT calculations. The choice of this functional form was guided by the requirement that $V(R,\theta)$ should correctly describe the topology of the PES (depth and location of the minima) and allow for rapid, repeated evaluations of $V(R,\theta)$ and derivatives required for MD simulations. The inaccuracies in the fitting are of similar order (or smaller) than the uncertainties from the DFT calculations.

Such low-dimensional potential energy functions are usually calculated without taking account of the protein environment. Thus, it is important to carry out test calculations for stationary points including the electrostatic environment provided by the protein. This can be done using QM/MM calculations. For MbNO it was shown that the general topology of the PES is not changed although the barriers between the stationary points may be different for the gas phase system compared with the situation in the protein [56]. Nevertheless, PESs such as equation (1) allow to investigate the dynamics in a complex environment in a more realistic fashion than is possible with a conventional force field.

### 3.3. *Vibrational spectroscopy*

Vibrational spectroscopy of small molecules can provide a detailed understanding of the (electrostatic and steric) environment surrounding that ligand. Thus, a dissociated ligand can be used as a local probe. For such investigations infrared and Raman spectroscopy can be used. In the case of MbCO much work has been carried out for both the bound (A) and unbound (B) states. Less is known about the infrared

spectroscopy of bound/unbound NO and $O_2$. From a computational point of view the infrared spectrum of a molecule can be directly related to the autocorrelation function of the dipole moment time series $\mu(t)$ [57]. Yet simpler, a normal mode analysis provides an approximate picture of the fundamental frequencies of the system [58]. This approach is covered in a number of recent publications [59–61]. Molecular dynamics simulations can also be used to follow energy flow and the rate of cooling after photodissociation of the ligand from the heme. Insightful investigations on energy redistribution in Mb have been carried out by Straub and coworkers [58, 62–64].

MD simulations provide positions of atoms at every time step along a trajectory. From the partial charges of the force field the total dipole moment $M(t)$ of an entire molecule or a relevant sub-group of atoms can be calculated. From this, the real-time dipole–dipole autocorrelation function, $C(t)$, is constructed. The infrared spectrum, $C(\omega)$, is calculated from the Fourier transform of the time correlation function $C(t) = \langle \mu(0)\mu(t) \rangle$ [57]. $C(t)$ is accumulated over $2^n$ time origins, where $n$ is an integer such that $2^n$ corresponds to between approximately 1/3 and 1/2 of the trajectory. This function can then be transformed using a Fast Fourier Transform with appropriate numerical filters to minimize noise [30]. The final infrared absorption spectrum is calculated by evaluating

$$A(\omega) = \omega\{1 - \exp[-\omega/(kT)]\}C(\omega), \tag{2}$$

where $k$ is the Boltzmann constant and $T$ is the temperature in Kelvin. Numerical experiments on simple systems have shown that the fundamental excitations calculated from the classical dipole–dipole correlation function do not exactly agree with solutions of the nuclear Schrödinger equation. In the case of CO, using the RRKR potential by Huffaker [65] gives $2144.6\,\mathrm{cm}^{-1}$ for the fundamental excitation ($2143.3\,\mathrm{cm}^{-1}$ from experiment) while calculating the fundamental from the Fourier transform of $C(t)$ gives $2183\,\mathrm{cm}^{-1}$. This is a shift of about $40\,\mathrm{cm}^{-1}$ between the quantum mechanically correct result and the frequency derived from the Fourier transform of the classical dipole autocorrelation function. Previous investigations of the infrared spectrum of photodissociated CO were based on electric field induced vibrational frequency shifts [66, 67]. While the analyses give insight into the overall Stark shift of the CO absorption and the location of CO after photodissociation, both studies are unable to reproduce the observed splitting of the CO infrared spectrum [16].

The averaged infrared spectrum of photodissociated CO in native Mb calculated from several trajectories is shown in figure 3 together with the experimental spectrum [16, 44]. The infrared spectrum of the dissociated CO reproduces the experimentally observed splitting of the peak corresponding to CO in the docking site. The origin of the splitting can be attributed to two different orientations of the CO molecule within the docking site, with the splitting in almost quantitative agreement with experiment. More recently, the time-resolved infrared spectrum and X-ray diffraction of photodissociated $^{13}CO$ in the L29F Mb mutant was measured [17]. In this mutant the leucine (L) residue at position 29 is replaced by a bulky phenylalanine

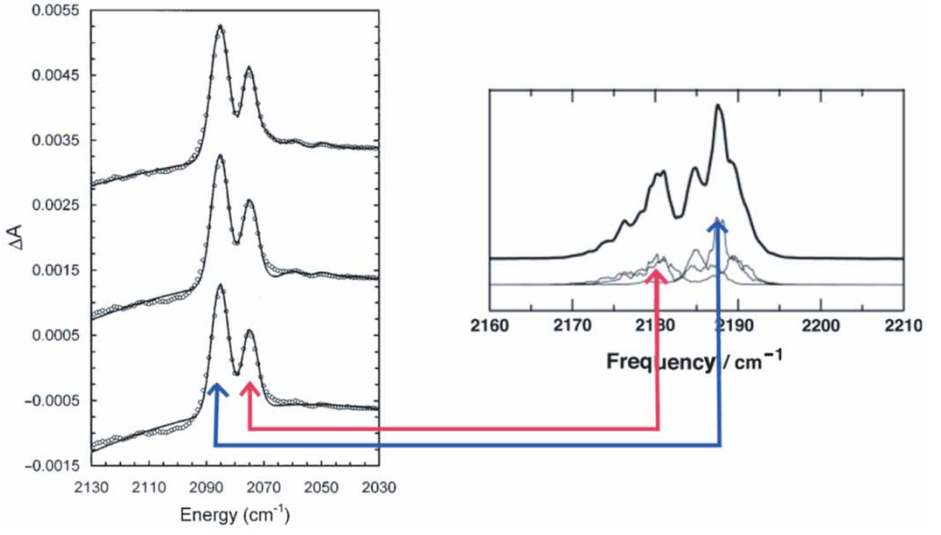


Figure 3. [Colour online] Experimental (left) [16] and calculated (right) [44] infrared spectrum of photodissociated CO from native Mb. The experimental spectrum is for $^{13}$CO while the calculated one is for $^{12}$CO. Note that the energy scales are running in opposite directions. The calculated infrared spectrum reproduces the two peaks observed experimentally, with a separation of 8 cm$^{-1}$, in close agreement with experiment.



(F) (see figure 1). In contrast to experiments on native Mb it was found that the characteristic infrared absorption band for CO changes profoundly in the case of the L29F mutant. The split infrared spectrum, indicative of the population of different states (e.g. conformational substates B1 and B2 which differ in the orientation of the CO [68, 69], and possibly B3, which can only be populated by extended illumination in native MbCO [70]) is fundamentally altered. For L29F the splitting in the infrared spectrum disappears after approximately 100 ps while it persists for 100 ns for native Mb.

Infrared spectra of CO in L29F calculated from a large number of 100 ps trajectories exhibit two peaks separated by $\approx$15 cm$^{-1}$. This corresponds favorably with the time-resolved spectra presented by Schotte *et al.* taken between 1 ps and 100 ps, which also show a dominant feature at higher wavenumbers and a smaller peak roughly 15 cm$^{-1}$ below [17]. The smaller peak disappears at longer observation times. Since experimentally a decaying peak with a time constant of 140 ps is observed, it is conceivable that the corresponding peak in the calculated spectrum should be smaller, as is found to be the case. For the spectra calculated from five 1 ns trajectories one single peak is obtained. This is also in agreement with experiments where, at longer time scales (>100 ps), a single signal appeared which was assigned to CO inside the protein matrix but *not* in the docking site at the edge of the distal heme pocket. For the L29F mutant the CO molecule escapes from the distal pocket on a time scale of a few ten to several hundred ps and diffuses into the neighbouring Xe4 pocket. The mutation at residue 29 sufficiently alters the nature of the docking site at the edge of the distal heme pocket to induce this change.

### 3.4. *Ligand migration and rebinding from around the active site*

The dynamics of photodissociated ligands – in particular CO and NO – have been the subject of intense experimental and theoretical work. Important questions concerning this process can be summarized as: *to where and on what time scale does the ligand diffuse and what observable properties are associated with this process?* Mutation experiments play an important role in these studies because particular mutations around the active site (e.g. V68L, V68A, H64L, L29W) [51, 71] have been shown to modify pathways within the protein. In different Mb mutants access to the internal Xe pockets is more or less facile or even completely blocked [51].

For MbCO the chemically bound state is typically referred to as the A state. The binding site (B) is of major importance since after photodissociation (MbCO → Mb···CO) it is rapidly populated. From there, the ligand can either rebind directly or follow a largely unknown path within the protein to diffuse towards the solvent from where it rebinds at much longer time scales [52, 72]. A pictorial representation of ligand diffusion in Mb is given in figure 4. One possible, secondary binding site in the neighborhood of site B is the Xe4 pocket [17, 21, 51, 52, 73]. For native Mb, experimental evidence for population of the Xe4 pocket by CO after dissociation appears to be sparse. It is only recently that FTIR-TDS experiments have found migration of photolysed CO from the primary docking site B to the Xe4 cavity [51]. This finding is supported by results from a 90 ns MD simulation of native Mb···CO which shows that CO occupies the Xe4 cavity before migrating further in the protein matrix [52], and by further, independent MD simulations [40, 44, 73]. Using time-resolved X-ray crystallography it has been found that the Xe4 pocket in the L29F mutant is populated within about 1 ns after photodissociation [17]. 3 ns after dissociation it is still populated while at 30 ns all CO molecules have moved out of the Xe4 pocket, either back to the docking site or further to cavities such as Xe1. For native Mb···CO the analysis of the data shows that the rebinding dynamics is non-exponential at low temperatures and extends over timescales ranging from ps to s. At longer time scales CO is expected to diffuse to sites further away from the heme and to escape to the solvent from where it rebinds at much slower rates [2, 74].



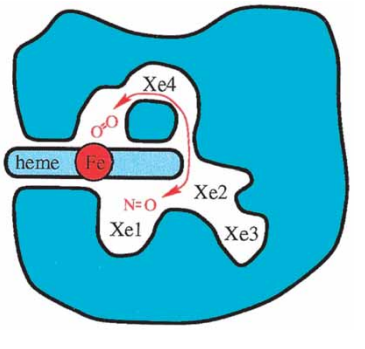


Figure 4. [Colour online] Qualitative representation of ligand diffusion in Mb (from [80]). The cross-section shows the positioning of the cavities and the heme plane relative to each other. His93 (see figure 1) binds from below (near the Xe1 pocket).

At room temperature the rebinding process becomes exponential in time with a rebinding constant of the order of 100 ns [2].

Experimentally, the rebinding dynamics of CO after photodissociation has been studied extensively for native Mb and for various mutants under different conditions [27, 75–77]. In the experiments one observes the number $N(t)$ of ligand molecules that have not rebound at time $t$ after photodissociation. Usually, rate constants ($k_{XY}$) are extracted by fitting a set of first order kinetic equations which describe transitions between stable and metastable states X and Y visited by the ligand during the rebinding dynamics [27, 51, 74, 76, 78]. For native and mutant MbCO three bound substates and a number of intermediate states after photodissociation have been identified directly and indirectly [27, 51, 79]. In many cases, the identity of the intermediate states (B, C, D) is not explicitly specified [74, 76, 78] but over the past few years evidence has been accumulated that B is the docking site and C is related to one of the internal Xe pockets [17, 27, 40, 80]. Recently, a sequential three-well model was convincingly fitted to rebinding data for the L29W mutant [27]. In this case, structural information was also available to correlate the metastable states with docking sites within the protein.



The rebinding of NO to Mb is much more rapid than for CO, and non-exponential at all temperatures [81]. Rapid and slow rebinding times ($\tau_r$ and $\tau_s$) vary between 28–280 ps and 5.3–133 ps depending on the experimental setup and the data analysis [81, 82]. Although all experiments on NO rebinding to Mb carried out to date agree on the existence of multiple time scales it is remarkable how much the results differ. Thus, the model for unravelling the underlying reaction scheme to interpret the data is important. A graphical representation of possible ligand pathways is sketched in figure 2 (see also [83]). After photodissociation the ligand diffuses to the docking site B and subsequently migrates *via* internal cavities (in an as yet largely unspecified sequence) to either escape into the solvent or geminately rebind from one of the internal cavities.

Complementary to the existence of secondary binding sites within Mb, it was suggested that heme relaxation may be involved in the observation of the non-exponential rebinding times. This hypothesis was captured in a remarkable theoretical model proposed by Agmon and Hopfield [84]. They considered two coordinates, a protein configuration coordinate $x$ and the Fe-ligand separation $r$, to describe a qualitative two-dimensional potential energy surface. Thus, the protein is treated with a single coordinate. This bounded diffusion model is a simple kinetic model which couples ligand migration ($r$) and protein relaxation ($x$) and allows to describe the transition from inhomogeneous (distributed rebinding barriers) to relaxation dominated kinetics. The model was recently refined and applied to a range of Mb mutants in different solvents [71]. In essence, the model solves the Smoluchowski equation subject to particular initial conditions and yields activation energies $E_D$ which describe the rebinding barrier. As an example, fitting the experimentally measured survival probability of photodissociated CO for native Mb in trehalose to the bounded diffusion model, $E_D = 6.5$ kcal/mol was found. This compares with $E_D = 4.3$ kcal/mol from an earlier application of a slightly modified theoretical model to wild type sperm whale Mb in trehalose [85]. Conversely, the classical study by Steinbach and coworkers found a conformationally averaged effective barrier $H_{eff} = 4.5$ kcal/mol for wild type

Mb at 300 K [75]. In an effort to generalize the Agmon and Hopfield model, Šrajer and coworkers have discussed an explicit dependence of the interaction potential on the heme-doming coordinate [47]. Using experimental constraints, model parameters were determined to best reproduce the measured kinetic data. These studies assumed a simplified, low-dimensional potential energy surface to describe the rebinding process. As studies on MbNO have shown, both effects (existence of secondary binding sites and distributed barriers due to internal relaxation) are likely to contribute to the observed rebinding dynamics [7]. In summary, the efforts described so far used reduced dimensionality (2D or 3D) models [47, 71, 84] to fit the survival probability after photodissociation or did not carry out the rebinding explicitly [7].

Recently, alternative approaches have been pursued to investigate the rebinding dynamics. They independently address two difficulties in all-atom simulations of ligand binding: the time scales involved and the description of chemical reactions in a force field-based framework.

*The timescale problem*: for rebinding of CO to Mb the timescales involved ($\approx 100$ ns) are still too long to collect meaningful statistics from atomistic simulations. One possibility to address this problem uses the Smoluchowski equation [86, 87] which is generally accepted to describe ligand diffusion in a protein matrix [71, 84, 88]. In one dimension $R$, diffusion is described as

$$\frac{\partial p(R,t)}{\partial t} = \frac{\partial}{\partial R} D(R) e^{-\beta G(R)} \frac{\partial}{\partial R} \left[ e^{\beta G(R)} p(R,t) \right]. \tag{3}$$

Equation (3) describes the decay of a non-equilibrium distribution $p(R, t = 0)$ to the equilibrium $p_{\mathrm{eq}}(R)$ governed by the free energy profile (FEP) $G(R)$ and a (position dependent) diffusion constant $D(R)$. To solve equation (3) the discrete approximation (DA) is used [89]. Depending on the roughness [90] of $G(R)$ computationally more efficient algorithms than the simple DA are available [91, 92].

The free energy profile $G(R)$ (which is also called potential of mean force (PMF)) can be calculated from MD simulations using umbrella sampling methods [31, 93]. In umbrella sampling, MD simulations are carried out to collect statistics $n_i$ for given intervals $\Delta\delta_i$ along a particular reaction coordinate $\delta$ using a biasing potential $V(\delta) = k_i(\delta - \delta_{0_i})^2$. Here, $k_i$ is the force constant and $\delta_{0_i}$ is the value around which the reaction coordinate should be restrained. Associated free energies $G(\delta)$ are extracted from $n_i$ via $f(i) = -kT \ln n_i + c$, after subtracting the biasing potential. Here, $k$ is the Boltzmann constant, $T$ is the temperature, and $c$ is an arbitrary constant. The constant $c$ is calculated as the value which minimizes the functional $\min\left[\sum_i (f_2(i) - f'_1(i))^2\right]$ in the overlap region $i$ of two adjoining windows. $f_1(j_1)$ and $f_2(j_2)$ are sets of points in the first and second interval and $f'_1(j_1) = f_1(j_1) - c$, respectively. In more than one dimension the preferred method to join statistics for adjoining windows is the weighted histogram method (WHAM) [94].

For the rebinding of a ligand to Mb two free energy surfaces are required: one for the bound state (MbCO) and one for the photodissociated state (Mb$\cdots$CO). Since the coupling in the crossing region is small [95] the two FESs can be diabatized and the lower diabat governs the rebinding reaction. The bound and unbound state dissociate to two different asymptotes and their energy difference $\Delta$ is only

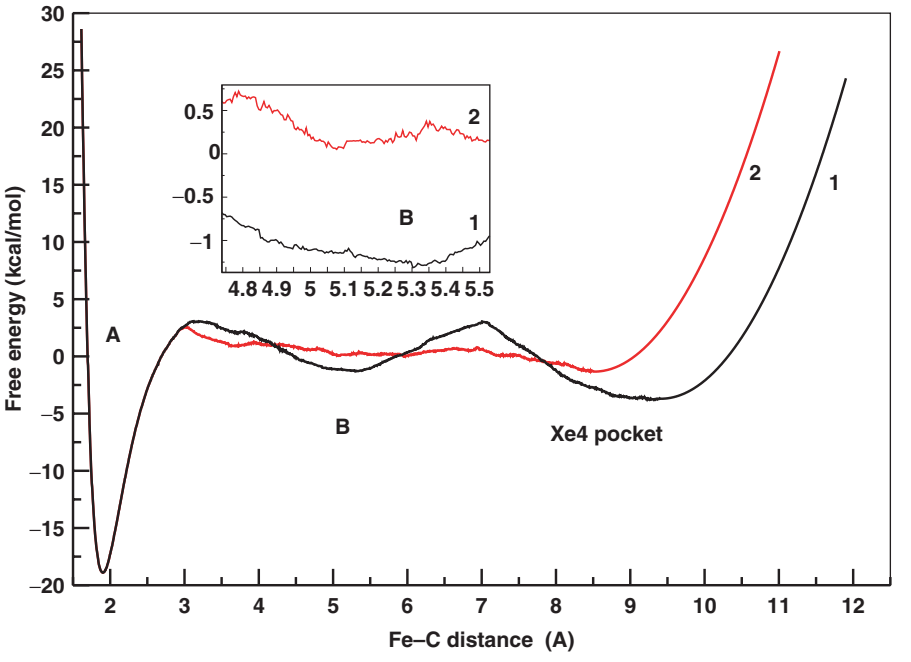


Figure 5. [Colour online] Free energy profile, $G(R)$, from umbrella sampling calculations for CO rebinding in native (Trace 1) and L29F mutant (Trace 2) Mb as a function of the distance $R$ between the heme-Fe and the carbon atom of CO. The inset shows the roughness of the FEP around the docking site B. Forward rates $k_{ij} = \exp[-\Delta G_{ij}/kT]$ are calculated for neighbouring points $x_i$ and $x_j$ to construct the rate matrix [91]. The profiles 1 and 2 are very different in their barriers which govern the rebinding dynamics.



known approximately. The value of $\Delta$ cannot be measured experimentally and only be calculated for model systems. As an example, in heme···CO it was estimated between 5 kcal/mol [96] and 10 kcal/mol [55]. Two examples for diabatized FESs are shown in figure 5. For native MbCO the FEP has two local minima, one for the ligand in the B site and one for the Xe4 pocket. The mutation L29F leads to a much flatter FEP. Solving the Smoluchowski equation for different initial conditions on the two FEPs leads to very rapid dynamics for the L29F mutant while rebinding for native MbCO occurs on timescales of several 10 to 100 ns, depending on the value of $\Delta$. Because for native Mb the inner barrier $H_{A\leftarrow B} = 4.3$ kcal/mol is lower than the outer barrier $H_{B\leftarrow Xe4} = 7.8$ kcal/mol, rebinding from Xe4 is much slower. Also, since for the forward barrier $H_{B\rightarrow Xe4} \approx H_{A\leftarrow B}$, population of the B state can equally well rebind to A and diffuse further away to Xe4 from where it rebinds on much longer timescales. For $\Delta = 4.0$ kcal/mol the experimentally observed $\tau = 100$ ns is found. $\Delta = 4.0$ kcal/mol gives an inner barrier of $H_{A\leftarrow B} = 4.3$ kcal/mol, in quite good agreement with an experimental estimate of $H_{eff} = 4.5$ kcal/mol [75]. On the other hand, the flat FEP for the L29F mutant supports the very rapid dynamics found in MD simulations [40] and in experiment [17].

It is important to note that, by construction, a FEP from umbrella sampling contains 'information' from all degrees of freedom of the protein. On the other hand, the technique of umbrella sampling may overestimate certain barriers because for each window the entire system is allowed to exhaustively sample low energy structures for the particular value of the driving coordinate. This can lead to local rearrangements on the time scales of the sampling (50 to 100 ps) which may not be possible in the experiment.

*Reactive molecular dynamics*: Even more fundamentally, there are no computationally feasible, accurate implementations of reactive molecular dynamics. As mentioned earlier, while QM/MM methods are an attractive method to investigate reactive processes in complex systems, the computational effort to cases in which many degrees of freedom are involved in the reaction itself becomes computationally prohibitive. On the other hand, approaches such as empirical valence bond (EVB) [38] or approximate valence bond theory (AVB) [39] require experimental data for fitting certain parameters of the model. Thus, a new methodology has been developed and extensively tested to follow the rebinding of NO to Mb after photodissociation. The 'reactive molecular dynamics' (RMD) method identifies a crossing of two multidimensional potential energy surfaces and carries out the crossing between the two PESs over a finite time window [97]. During the crossing, energy and force terms are mixed and smoothly varied between the two energy manifolds. At the end of a crossing (which typically occurs over 10 fs) the system has moved from one PES to the other. Importantly, recrossings are also possible. This can be seen in figure 6 where a trajectory starting on the unbound state (blue trace) close to a configuration of the Fe–ON metastable state crosses (A) to the bound state surface (red trace) and relaxes



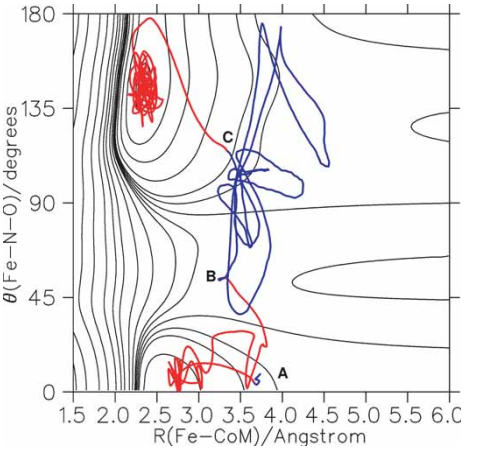


Figure 6. Rebinding trajectory, from reactive molecular dynamics simulations [97], of photodissociated NO from native Mb projected onto the two-dimensional bound state MbNO potential energy surface. The trajectory starts on the unbound state (blue, position A). After a few time steps a crossing between the bound and the unbound PES is found and the trajectory continues on the bound state PES (red). After sampling the Fe–ON configuration ($\theta = 0$), a crossing is found (B) in an approximately T-shaped Fe–ON conformation and the trajectory crosses to the unbound state. Extensive sampling of the unbound state leads to a final crossing (C) and relaxation into the global Fe–NO minimum follows.

into the Fe–ON minimum. Through energy exchange the system is allowed to reach the transition state region between Fe–ON and Fe–NO (the global minimum) and recrosses (B) to the unbound state. After a considerable time the trajectory finds another crossing (C) to the bound state surface after which it finally relaxes into the Fe–NO minimum.

Because the rebinding of NO to Mb occurs on much faster time scales [81, 82] (ps time range) than the one for CO [75], MbNO is an ideal test system for explicit rebinding simulations. An analysis of several thousand trajectories established that the rebinding probability $p(t)$ as a function of the time $t$ after photodissociation is nonexponential in time, in agreement with experiment and previous simulations [2, 7, 81, 82]. The time constants from a double exponential fit are 3.8 and 18.0 ps (see figure 7) which is in qualitative agreement with experiments, which yield 28 and 280 ps [81] or 5.3 and 133 ps [82]. For the unbound state the fluctuating three-point charge model was used [98] while for the bound state a two-dimensional PES for the interaction between heme and NO is available [56]. As for MbCO, the asymptotic separation $\Delta$ between the bound and the unbound potential energy manifold is unknown and treated as a parameter. The simulations suggest that the observed nonexponential rebinding dynamics of NO to Mb is governed by a time-dependent rebinding barrier at short times after dissociation while at longer times a distribution of potential energy barriers due to the occupation of several locations within the protein arise.



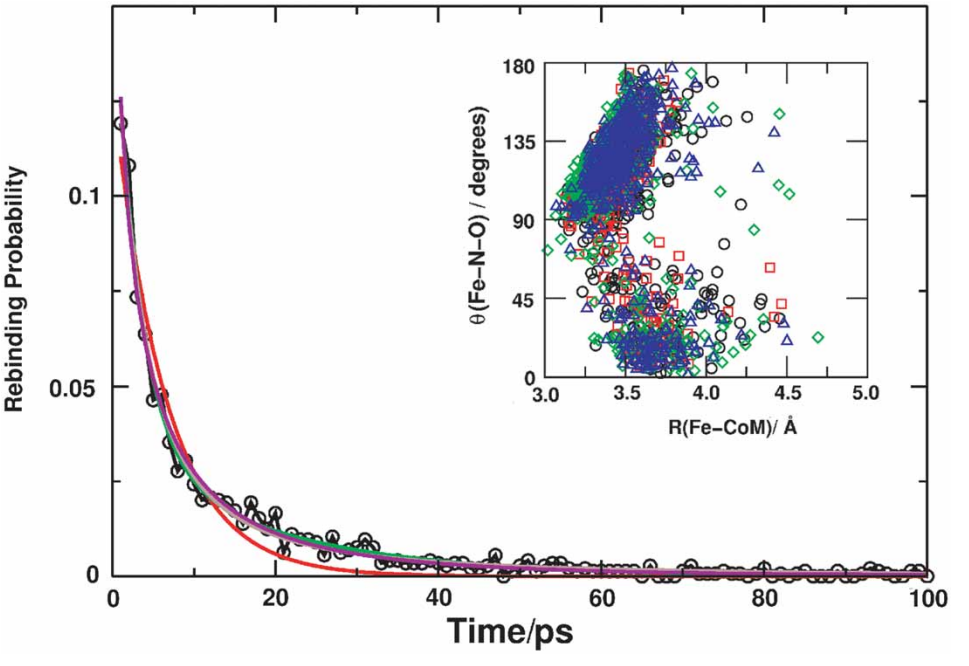


Figure 7. Statistics on the rebinding probability from 6000 rebinding trajectories [97]. A single exponential fit (red) can not reproduce the rebinding probability, while a two-exponential, a stretched exponential, or a power-law all fit equally well. The inset shows the distribution of recrossing geometries as a function of the Fe–CoM(NO) separation and the Fe–NO angle.

In addition to the time course of the rebinding reaction it is also possible to investigate other aspects of chemical reactions. For example, it is interesting to analyse the 'reactive configurations' of a high dimensional system. For this, the Fe-ligand centre of mass separation and the Fe–NO angle at the crossing points are considered. Figure 7 shows that the rebinding reaction from the bound to the unbound state (or vice versa) in MbNO is characterized by a wide seam. Thus, there is a large number of 'reactive configurations' although the majority of reactive events occurs near the minima of the bound PES.

## 4. Conclusion and outlook

Even almost 50 years after the solution of the X-ray structure and the first flash photolysis experiments, myoglobin remains an interesting and challenging protein to investigate. Over the years it has developed into a model system for chemists, physicists, biologists and researchers working at the interfaces of these disciplines. Many intrinsic properties of proteins (flexibility, ligand recognition, catalysis, regulation of activity) have been observed in myoglobin which provided a wealth of experimental data. Because of this, myoglobin is nowadays one of the first systems to which new experimental and theoretical techniques are applied. One recent example is time-resolved X-ray crystallography [17, 99].

One of the challenges to theory and experiment alike is to provide a coherent picture of the inner workings of myoglobin (together with its ligands) over wide temperature (few K to 300 K) and time (fs to s) ranges. Paramount to computational studies will be the development of new and refinement of established techniques to address the problems that have been highlighted in the present work. As has become clear, the close collaboration between experiment and simulation can provide the details necessary to understand one of the best characterized proteins [58, 100]. Furthermore, computer simulations including all degrees of freedom, preferentially carried out in full solvation (water and other solvents) over long time scales will add to our understanding of ligand migration in Mb.

Until now, the application of dedicated numerical methods has shed light on the metastable structure of photodissociated CO, the infrared spectroscopy of dissociated CO (split line) and NO (no splitting), and the time course of the rebinding reaction using either coarse grained (Smoluchowski) models or explicit rebinding dynamics simulations. Much more remains to be discovered and understood and there are numerous opportunities for meaningful, dedicated and accurate computational investigations. Challenging questions concern the detailed understanding of the selectivity of Mb of $O_2$ over CO including the dynamics of ligand entry into the protein, or the function of Mb within Hb (which is a tetrameric hemeprotein with a heme prosthetic group identical to that of myoglobin). On the very rapid time scale (femtoseconds), the interplay of electronic and nuclear degrees of freedom during the photodissociation event, is poorly understood and presents a real challenge in non-adiabatic reaction dynamics [101]. Finally, the observation of low frequency heme-modes [102] presents an ideal opportunity to refine the force fields and to further investigate energy flow within Mb [64].

## Acknowledgments

We gratefully acknowledge financial support from the Schweizerischer Nationalfonds which supports the present research through a Förderungsprofessur to M.M. Generous allocation of computing time at the CSCS in Manno, Switzerland, is acknowledged.

## References

[1] J. C. Kendrew, G. Bodo, H. M. Dintzis, P. G. Parrish, H. Wyckoff, and D. C. Philipps, Nature **161,** 662 (1958).
[2] R. Austin, K. Beeson, L. Eisenstein, H. Frauenfelder, and I. Gunsalus, Biochem. **14,** 5355 (1975).
[3] J. A. McCammon and S. C. Harvey, *Dynamics of Proteins and Nucleic Acids* (Cambridge University Press, Cambridge, 1987).
[4] M. Brunori and Q. H. Gibson, EMBO Rep. **2,** 674 (2001).
[5] E. R. Henry, M. Levitt, and W. A. Eaton, Proc. Natl. Acad. Sci. **82,** 2034 (1985).
[6] R. Elber and M. Karplus, Science **235,** 318 (1987).
[7] M. Meuwly, O. M. Becker, R. Stote, and M. Karplus, Biophys. Chem. **98,** 183 (2002).
[8] G. B. Richter-Addo, P. Legzdins, and J. Burstyn, Chem. Rev. **102** (2002).
[9] T. Dawson, V. Dawson, and S. Snyder, Ann. Neurology **32,** 297 (1992).
[10] S. Snyder and D. Bredt, Scientific American **May**, 68 (1992).
[11] T. Traylor and V. Sharma, Biochem. **31,** 2847 (1992).
[12] Q. H. Gibson and M. H. Smith, J. Physiol. **136,** P27 (1957).
[13] Q. H. Gibson, J. Physiol. **134,** 123 (1956).
[14] P. Cornelius, R. Hochstrasser, and W. Steele, J. Mol. Biol. **163,** 119 (1983).
[15] P. A. Anfinrud, C. Han, and R. Hochstrasser, Proc. Natl. Acad. Sci. **86,** 8387 (1989).
[16] M. Lim, T. A. Jackson, and P. A. Anfinrud, J. Chem. Phys. **102,** 4355 (1995).
[17] F. Schotte, M. Lim, T. A. Jackson, A. V. Smirnov, J. Soman, J. S. Olson, G. N. Phillips Jr, M. Wulff, and P. A. Anfinrud, Science **300,** 1944 (2003).
[18] W. D. Tian, J. T. Sage, V. Šrajer, and P. M. Champion, Phys. Rev. Lett. **68,** 408 (1992).
[19] K. Moffat, Chem. Rev. **101,** 1569 (2001).
[20] D. C. Lamb, K. Nienhaus, A. Arcovito, F. Draghi, A. E. Miele, M. Brunori, and G. U. Nienhaus, J. Biol. Chem. **277,** 11636 (2002).
[21] R. F. Tilton Jr, I. D. Kuntz Jr, and G. A. Petsko, Biochem. **23,** 2849 (1984).
[22] A. D. MacKerell Jr, D. Bashford, M. Bellott, R. L. Dunbrack Jr, J. D. Evanseck, M. J. Field, S. Fischer, J. Gao, H. Guo, S. Ha, D. Joseph-McCarthy, L. Kuchnir, K. Kuczera, F. T. K. Lau, C. Mattos, S. Michnick, T. Ngo, D. T. Nguyen, B. Prodhom, W. E. Reiher III, B. Roux, M. Schlenkrich, J. C. Smith, R. Stote, J. E. Straub, M. Watanabe, J. Wiorkiewicz-Kuczera, D. Yin, and M. Karplus, J. Phys. Chem. B **102,** 3586 (1998).
[23] S. J. Weiner, P. A. Kollman, D. A. Case, U. Singh, C. Ghio, G. Alagona, S. Profeta Jr, and P. Weiner, J. Am. Chem. Soc. **106,** 765 (1984).
[24] J. Hermans, H. J. C. Berendsen, W. F. van Gunsteren, and J. P. M. Postma, Biopol. **23,** 1 (1984).
[25] W. L. Jorgensen and J. Tirado-Rives, J. Am. Chem. Soc. **110,** 1657 (1988).
[26] C. F. Lopez, S. O. Nielsen, P. B. Moore, and M. L. Klein, Proc. Natl. Acad. Sci. **101,** 4431 (2004).
[27] A. Ostermann, R. Waschipky, F. G. Parak, and G. U. Nienhaus, Nature **404,** 205 (2000).
[28] W. L. Jorgensen and J. Tirado-Rives, Proc. Natl. Acad. Sci. **102,** 6665 (2005).
[29] M. Karplus and J. Kuriyan, Proc. Natl. Acad. Sci. **102,** 6679 (2005).
[30] M. P. Allen and D. J. Tildesley, Computer Simulation of Liquids, (Clarendon Press, Oxford, 1989).
[31] J. Kottalam and D. A. Case, J. Am. Chem. Soc. **110,** 7690 (1988).
[32] M. Mezei, J. Chem. Phys. **86,** 7084 (1987).
[33] A. Warshel and M. Levitt, J. Mol. Biol. **103,** 227 (1976).
[34] G. Alagona, C. Guio, and P. A. Kollman, J. Mol. Biol. **191,** 23 (1986).
[35] P. A. Bash, M. J. Field, and M. Karplus, J. Am. Chem. Soc. **109,** 8092 (1987).
[36] R. A. Friesner and V. Guallar, Ann. Rev. Phys. Chem. **56,** 389 (2005).
[37] M. J. Field, P. A. Bash, and M. Karplus, J. Comp. Chem. **11,** 700 (1990).
[38] A. Warshel and R. M. Weiss, J. Am. Chem. Soc. **102,** 6218 (1980).
[39] P. Grochowski, B. Lesyng, P. Bala, and J. A. McCammon, Int. J. Quant. Chem. **60,** 1143 (1996).

[40] D. R. Nutt and M. Meuwly, Proc. Natl. Acad. Sci. **101,** 5998 (2004).
[41] R. Car and M. Parrinello, Phys. Rev. Lett. **55,** 2471 (1985).
[42] S. Patel and C. L. Brooks, J. Chem. Phys. **122,** 024508 (2005).
[43] G. Maroulis, Chem. Phys. Lett. **334,** 214 (2001).
[44] D. R. Nutt and M. Meuwly, Biophys. J. **85,** 3612 (2003).
[45] I. Schlichting, J. Berendzen, G. N. Phillips, and R. M. Sweet, Nature **371,** 808 (1994).
[46] T. Y. Teng, V. Šrajer, and K. Moffat, Nature Structural Biology **1,** 701 (1994).
[47] V. Šrajer, L. Reinisch, and P. Champion, J. Am. Chem. Soc. **110,** 6656 (1988).
[48] J. E. Straub and M. Karplus, Chem. Phys. **158,** 221 (1991).
[49] D. Vitkup, G. A. Petsko, and M. Karplus, Nature Structural Biology **4,** 202 (1997).
[50] J. Meller and R. Elber, Biophys. J. **74,** 789 (1998).
[51] K. Nienhaus, P. Deng, J. M. Kriegl, and G. U. Nienhaus, Biochem. **42,** 9647 (2003).
[52] C. Bossa, A. Massimiliano, D. Roccatano, A. Amadei, B. Vallone, M. Brunori, and A. Di Nola, Biophys. J. **86,** 3855 (2004).
[53] O. Schaad, H.-X. Zhou, A. Szabo, W. A. Eaton, and E. R. Henry, Proc. Natl. Acad. Sci. **90,** 9547 (1993).
[54] H. Li, R. Elber, and J. E. Straub, J. Biol. Chem. **268,** 17908 (1993).
[55] B. H. McMahon, B. P. Stojković, J. P. Hay, R. L. Martin, and A. E. García, J. Chem. Phys. **113,** 6831 (2000).
[56] D. R. Nutt, M. Karplus, and M. Meuwly, J. Phys. Chem. B **109,** 21118 (2005).
[57] D. A. McQuarrie, *Statistical Mechanics*, (Harper & Row, New York, 1976).
[58] D. E. Sagnella, J. E. Straub, T. A. Jackson, M. Lim, and P. A. Anfinrud, Proc. Natl. Acad. Sci. **96,** 14324 (1999).
[59] F. Tama, F. X. Gadea, O. Marques, and Y. H. Sanejouand, Prot. Struct. Funct. Genom. **41,** 1 (2000).
[60] G. H. Li and Q. Cui, Biophys. J. **83,** 2457 (2002).
[61] I. Bahar and A. J. Rader, Curr. Op. Struct. Biol. **15,** 586 (2005).
[62] D. E. Sagnella, J. E. Straub, and D. Thirumalai, J. Chem. Phys. **113,** 7702 (2000).
[63] D. E. Sagnella and J. E. Straub, J. Phys. Chem. B **105,** 7057 (2001).
[64] L. Mu and J. E. Straub, J. Phys. Chem. B **107,** 10634 (2003).
[65] J. N. Huffaker, J. Chem. Phys. **64,** 3175 (1976).
[66] J. Ma, S. Huo, and J. E. Straub, J. Am. Chem. Soc. **119,** 2541 (1997).
[67] J. Meller and R. Elber, Biophys. J. **74,** 789 (1998).
[68] M. Lim, T. A. Jackson, and P. A. Anfinrud, J. Chem. Phys. **102,** 4355 (1995).
[69] M. Lim, T. A. Jackson, and P. A. Anfinrud, Nature Structural Biology **4,** 209 (1997).
[70] G. U. Nienhaus, J. R. Mourant, K. Chu, and H. Frauenfelder, Biochem. **33,** 13413 (1994).
[71] D. Dantsker, U. Samuni, J. M. Friedman, and N. Agmon, Bioch. Bioph. Acta **1749,** 234 (2005).
[72] R. Elber and M. Karplus, J. Am. Chem. Soc. **112,** 9161 (1990).
[73] P. Banushkina and M. Meuwly, J. Phys. Chem. B **109,** 16911 (2005).
[74] J. Olson and G. Philipps, J. Biol. Chem. **271,** 17593 (1996).
[75] P. J. Steinbach, A. Ansari, J. Berendzen, D. Braunstein, K. Chu, B. R. Cowen, D. Ehrenstein, H. Frauenfelder, J. B. Johnson, D. C. Lamb, S. Luck, J. R. Mourant, G. U. Nienhaus, P. Ormos, R. Philipp, A. Xie, and R. D. Young, Biochem. **30,** 3988 (1991).
[76] A. Ansari, C. M. Jones, E. R. Henry, J. Hofrichter, and W. A. Eaton, Biochem. **33,** 5128 (1994).
[77] V. Šrajer, Z. Ren, T. Y. Teng, M. Schmidt, T. Ursby, D. Bourgeois, C. Pradervand, W. Schildkamp, M. Wulff, and K. Moffat, Biochem. **40,** 13802 (2001).
[78] T. E. Carver, R. J. Rohlfs, J. S. Olson, Q. H. Gibson, R. S. Blackmore, B. A. Springer, and S. G. Sligar, J. Biol. Chem. **265,** 20007 (1990).
[79] J. Vojtechovsky, K. Chu, J. Berendzen, R. B. Sweet, and I. Schlichting, Biophys. J. **77,** 2153 (1999).
[80] H. Frauenfelder, B. J. McMahon, R. H. Austin, K. Chu, and J. T. Groves, Proc. Natl. Acad. Sci. **98,** 2370 (2001).
[81] J. W. Petrich, J.-C. Lambry, K. Kuczera, M. Karplus, C. Poyart, and J.-L. Martin, Biochem. **30,** 3975 (1991).
[82] S. Kim, G. Jin, and M. Lim, J. Phys. Chem. B **108,** 20366 (2004).
[83] M. Brunori, D. Bourgeois, and B. Vallone, J. Struct. Biol **147,** 223 (2004).
[84] N. Agmon and J. Hopfield, J. Chem. Phys. **79,** 2042 (1983).
[85] G. M. Sastry and N. Agmon, Biochem. **36,** 7097 (1997).
[86] M. Smoluchowski, Ann. Phys. **21,** 756 (1906).
[87] M. Smoluchowski, Ann. Phys. **1103,** 1915 (1915).
[88] A. Ansari, J. Chem. Phys. **112,** 2516 (2000).
[89] D. Bicout and A. Szabo, J. Chem. Phys. **109,** 2325 (1998).
[90] R. Zwanzig, Proc. Natl. Acad. Sci. **85,** 2029 (1988).
[91] P. Banushkina and M. Meuwly, J. Chem. Theo. Comp. **1,** 208 (2005).

[92] P. Banushkina, O. Schenk, and M. Meuwly, Lecture Notes in Bioinformatics **3695,** 208 (2005).
[93] G. M. Torrie and J. P. Valleau, J. Chem. Phys. **23,** 187 (1977).
[94] S. Kumar, D. Bouzida, R. H. Swendsen, P. A. Kollman, and J. M. Rosenberg, J. Comp. Chem. **13,** 1011 (1992).
[95] H. Frauenfelder and P. G. Wolynes, Science **229,** 337 (1985).
[96] J. N. Harvey, J. Am. Chem. Soc. **122,** 12401 (2000).
[97] D. R. Nutt and M. Meuwly, Biophys. J. **90,** 1191 (2006).
[98] D. R. Nutt and M. Meuwly, Chem. Phys. Chem. **5,** 1710 (2004).
[99] V. Šrajer, T. Teng, T. Ursby, C. Pradervand, Z. Ren, S. Adachi, W. Schildkamp, D. Bourgeois, M. Wulff, and K. Moffat, Science **274,** 1726 (1996).
[100] G. Hummer, F. Schotte, and P. A. Anfinrud, Proc. Natl. Acad. Sci. **101,** 15330 (2004).
[101] X. Ye, A. Demidov, and P. M. Champion, J. Am. Chem. Soc. **124,** 5914 (2002).
[102] Y. Mizutani and T. Kitagawa, Science **278,** 443 (1997).
[103] E. E. Scott and Q. H. Gibson, Biochem. **36,** 11909 (1997).
[104] E. E. Scott, Q. H. Gibson, and J. S. Olson, J. Biol. Chem. **276,** 5177 (2001).